Model Wind Turbines Tested at Full-Scale Similarity

M.A. Miller[1], J. Kiefer[2] C. Westergaard[3] and M. Hultmark[4]

[1,2,4]Mechanical and Aerospace Engineering, Princeton University, Princeton, NJ, USA
[3]Department of Mechanical Engineering, Texas Tech University, Lubbock, TX, USA

E-mail: [1]millerma@princeton.edu, [2]jkiefer@princeton.edu,
[3]carsten.westergaard@ttu.edu, [4]hultmark@princeton.edu

Abstract. The enormous length scales associated with modern wind turbines complicate any efforts to predict their mechanical loads and performance. Both experiments and numerical simulations are constrained by the large Reynolds numbers governing the full-scale aerodynamics. The limited fundamental understanding of Reynolds number effects in combination with the lack of empirical data affects our ability to predict, model, and design improved turbines and wind farms. A new experimental approach is presented, which utilizes a highly pressurized wind tunnel (up to 220 bar). It allows exact matching of the Reynolds numbers (no matter how it is defined), tip speed ratios, and Mach numbers on a geometrically similar, small-scale model. The design of a measurement and instrumentation stack to control the turbine and measure the loads in the pressurized environment is discussed. Results are then presented in the form of power coefficients as a function of Reynolds number and Tip Speed Ratio. Due to gearbox power loss, a preliminary study has also been completed to find the gearbox efficiency and the resulting correction has been applied to the data set.

1. Introduction

The large size of modern wind turbines makes it extremely challenging to perform resolved numerical simulations or model scale experiments at relevant conditions–such experiments have even been referred to as impossible. Past laboratory-scale experiments have been limited in their scope due to the difficulty of matching the three important, fluid mechanics related, non-dimensional parameters simultaneously ([1, 2, 3, 4]). These parameters are the Reynolds number, $Re = \frac{UL}{\nu}$, the Tip Speed Ratio, $TSR = \frac{\Omega L}{U}$, and the Mach Number, $Ma = \frac{U}{a}$. Here, U is the characteristic velocity, L the relevant length-scale, Ω the turbine's angular velocity, a the local speed of sound, and ν the kinematic viscosity. By matching these parameters simultaneously, while also retaining geometric similarity, one has obtained full dynamic similarity to the flow of the full scale turbine. Typically, an experimentalist only has control over the size of the model turbine (which is limited by the physical tunnel size), its rotation rate and the fluid velocity. In a conventional wind tunnel (or even water channel), all three parameters cannot be simultaneously matched. The NREL/NASA Ames Phase IV Unsteady Aerodynamics Experiments [5] or the MEXICO Tests [6] bypassed this problem by keeping the model scale ratio low, using very large wind tunnels. However, such experiments are very expensive, and if one wants to study the detailed wake evolution, even larger wind tunnels are required.

This report outlines a unique method of performing laboratory experiments which match the full-scale flow parameters while retaining geometric similarity, and thus capturing the full

scale fluid dynamics. By testing in a specialized high-pressure wind tunnel, known as the High-Reynolds number Test Facility (HRTF), the density of the air inside the tunnel can be varied from 1 to greater than 200 times atmospheric density. Since the dynamic viscosity, μ, is only a weak function of pressure, the Reynolds number can be increased by a factor of almost 200 without increasing the velocity. Furthermore, with this wind tunnel the Reynolds number may be adjusted independently of the Mach Number and Tip Speed Ratio by simply varying the tunnel pressure and hence achieve full-dynamic similarity with a wind turbine despite the small physical size of the model.

2. Experiment Description

Matching the full-scale Reynolds numbers on a small-scale model brings with it a host of challenges related to the large loads placed on the model and test setup. Both aerodynamic forces and torques scale with the fluid density:

$$F \propto \rho U^2 \pi R^2 \qquad \tau \propto \rho U^3 \pi R^2 / \omega \tag{1}$$

Therefore the density increase inside the pressurized HRTF multiplies both the aerodynamic forces, F, and torques, τ, by factors up to 200 times over that which would be seen by the model in an atmospheric wind tunnel at the same velocity. For instance, a turbine operating at a $C_t = 1.2$ and $C_p = 0.6$ would produce over 400 Newtons in thrust and 2 Kilowatts in power. This creates considerable design challenges when creating a model rotor and gearbox which have strict definitions of the external geometry due to the requirement of geometric similarity. In this work, careful consideration has been given to designing a robust system which can withstand the aerodynamic loading and provide accurate measurements of the power and thrust.

2.1. High Reynolds Number Test Facility (HRTF)

The High Reynolds Number Test Facility (HRTF) is a recirculating-type, low-speed, high-pressure wind tunnel which uses air as the working fluid. The facility is designed to support pressures up to 24 MPa (3500 PSI, or in excess of 230 atmospheres) and free-stream velocities in the test section of up to 10 m/s. The free-stream velocity is sampled upstream of the wind turbine model using a fixed pitot-static tube. The pressure differential is measured with a Validyne DP-15 differential pressure transducer with a range of 3447.4 $\pm$ 8.62 (Pa) (0.5 $\pm$ 0.00125 PSI). The test section itself is 4.88 meters (16 feet) long with an inside diameter of 48.9 cm (19.25 inches). It is preceded by a contracting section with an area ratio of 2.43:1. Before the contraction are a series of flow conditioning screens and honeycomb straighteners. This facility has been used in previous work concerning submarine wakes [7, 8, 9] and turbulent boundary layers [10]. The HRTF is shown in figure 1.

Figure 1. The High Reynolds Number Test Facility (HRTF) at the Princeton Gas Dynamics Laboratory. Direction of flow is clockwise from above.

2.2. Wind Turbine Model Geometry

The current experimental configuration utilizes a wind turbine rotor with a simplistic geometry. This makes the model freely available, straightforward to manufacture, and easy to reproduce for numerical simulations. Using this model, Reynolds number based on tip chord, $Re_c = \frac{c\sqrt{U^2+(\omega R)^2}}{\nu}$ values up to 3.5 million and $Re_D = \frac{UD}{\nu}$ values up to 20 million are possible in the HRTF. The model has a blockage ratio of $\beta = 16.7\%$ when used inside the HRTF. The blade geometry of the model is given in table 1. The hub geometry consists of a NACA 1 series spinner. The spinner geometry was copied from table I in [11] and scaled to the appropriate size for the wind turbine model.

Table 1. Wind turbine rotor model geometry with linear twist between sections 2 and 3

Section	Radius (mm)	Chord (mm)	Twist (degrees)	Airfoil
1	3.704	3.704	13	Circular
2	14.815	9.630	13	NACA 0035
3	100	3.704	0	NACA 0014

To ensure a very high tolerance on the surface finish and dimensional accuracy, the model is machined on a five axis Computer Numerical Control milling machine from a solid block of stainless steel. The model was measured for surface roughness, and it was found to be less than $k_{RMS} < 0.25$ (μm). For comparison, a Vestas V27 turbine, which operates at similar Reynolds number, has roughly one order of magnitude larger roughness on its surface when scaled with the turbine radius compared with the model.

2.3. Model Tower and Gearbox Design

The basic wind turbine model calls for a tower which can sustain the loads transfered to it with minimal deflection and with minimal intrusion into the flow. The loads include both aerodynamic thrust and torque imposed by the spinning rotor. To estimate the design space of the model in the HRTF, a series of Blade Element Momentum (BEM) simulations were carried out with the open-source Q-blade software, which has been validated against other BEM solvers in [12] and includes integrated XFOIL/XFLR5 functionality to solve for lift and drag polars. The geometry given in table 1 was used to compute the polars at various Reynolds numbers, which were in turn used to solve for the thrust load and power output. The results of these simulations are shown in figure 2. Note that these simulations were coarsely solved at individual Reynolds numbers and TSRs in order to estimate the maximum loads on the tower. Current work is ongoing to improve these simulations for comparison to the actual experiments.

Using these design loads as input to a set of free-body diagrams consisting of the gearbox input/output shaft, bearings, and bevel gears; a system of equations for the reaction loads were found following [13]. The design was constrained by a maximum outside width of 17 (mm) at the nacelle to minimize frontal blockage. This gives a ratio of frontal width to turbine diameter of $17/200 = 0.085$ which is very close to the value of the Vestas V27 manufacturer data (0.052) ensuring that the tower is of the same geometric scale as the rotor. Based on this constraint, the maximum allowable torque which could be sustained by this gearbox would be 1 (Nm) using a conservative Modified-Goodman factor of safety of 1.25. This torque limitation on the gearbox is unfortunate since the operating envelope of the model is clearly much larger at high Reynolds numbers. A second, improved gearbox design is currently being investigated to allow access to this larger Reynolds number and low tip speed ratio regime.

Following the design of the internal components, the resulting loads were then applied to a finite-element model of the tower itself using PTC CREO Simulate as shown in figure 3. Following several design iterations on the external tower geometry, the final tower is shown in

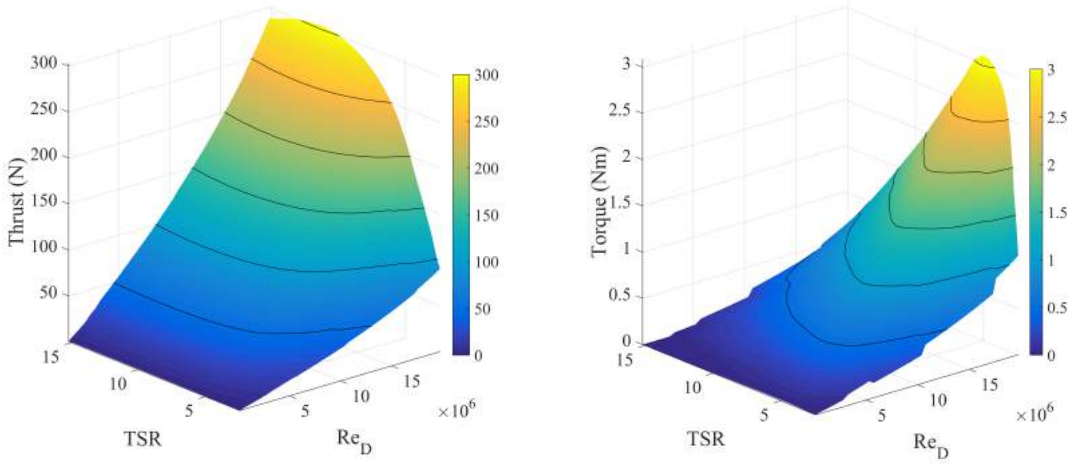

Figure 2. Preliminary blade element momentum simulations of thrust load and shaft torque versus Reynolds number and Tip Speed Ratio.

figure 4. To withstand the loads at higher torque and thrust values, high-strength steel was used to manufacture the tower. Currently the design is limited by the gear tooth material, as the maximum yield strength is surpassed around 1 (Nm). The tower itself was designed to withstand up to 3 (Nm) of shaft torque loading and over 300 (N) of axial thrust loading while minimizing the largest deflections to less than 400 microns.

Figure 3. Finite-element results showing von-Mises stress for lightly-loaded case (1 Nm input torque).

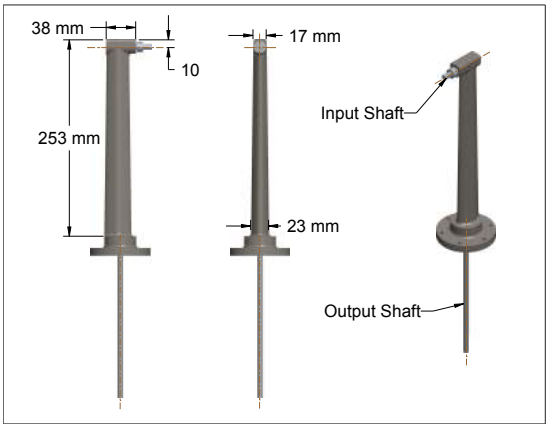

Figure 4. Overview of finalized tower geometry with input and output shafts shown.

2.4. Wind Turbine Measurement Stack

In order to facilitate accurate measurements of the loads applied to the wind turbine model and control the rotational speed, a measurement stack was designed and built to interface with the HRTF. This setup is shown in figure 5. The aerodynamic torque generated by the rotor is

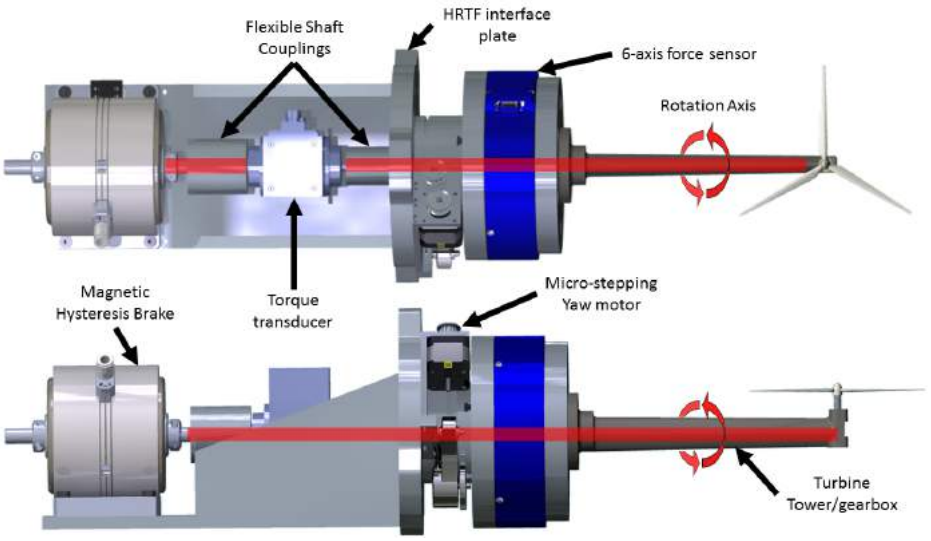

Figure 5. Schematic of wind turbine measurement stack. Note that the gearbox drive-shaft follows the rotation axis.

passed into a right-angle bevel gearbox located inside the turbine tower. This high-speed gearbox transfers the power onto the rotational axis of the measurement stack where it is passed, via the main drive-shaft, through the force sensor and rotary table and into the torque transducer. This torque sensor is a non-contact, rotary type (model TM-308 manufactured by Magtrol, Inc). This unit possesses a high stated accuracy of $< 0.1\%$ over the full range of 20 Newton-meters, while being able to resolve the torque signal at a sampling frequency of $f_s = 5,000\ (Hz)$. In future studies, this will allow for resolution of the torque signal by rotation. The torque transducer also measures the rotational speed via an internal optical encoder. After passing through the torque transducer, the power is removed from the system by a magnetic hysteresis brake (model AHB-3 manufactured by Magtrol, Inc). The brake allows for precise torque application, which is independent of rotational speed, and full control over the braking load applied to the turbine.

In order to resolve the forces acting on the turbine tower, a 6-axis force sensor (F_x, F_y, F_z, M_x, M_y, and M_z) is installed at the turbine tower base (model 75E20A4 manufactured by JR3 Inc). The measurement stack is designed so that all loads applied to the turbine must pass through the force sensor, with the exception of the shaft torque. Unfortunately, due to complications with the setup the current experiments were unable to capture the thrust coefficients. See table 2 for a list of the system accuracies.

Table 2. System Measurement Accuracy

Measurement	Range	Nominal Accuracy	Max. Sampling Frequency
$Torque,\ \tau$	20 (Nm)	$\pm$ 0.02 (Nm)	5 (kHz)
$Thrust,\ F_x$	1000 (N)	$\pm$ 2.5 (N)	500 (Hz)

3. Measuring Gearbox Efficiency

As described above, a small right-angle bevel gearbox is used to transfer the rotor torque out of the tunnel for measurement, see figure 6. It is therefore crucial to accurately predict the gearbox efficiency so that the aerodynamic torque can be determined. To this end, a test rig

was constructed outside of the HRTF which replicates the loads seen by the gearbox using a variable frequency drive, alternating current (AC) motor. The test rig is shown in the "gearbox test configuration" in figure 7. Here, a load is applied while the unit is rotating at a set speed and the torque is measured after passing through the gearbox. The test rig has a second configuration, not shown here, in which the gearbox is removed and the torque transducer/brake are connected directly to the AC motor. This allows for determination of the motor torque (τ_{motor}) as a function of rotational speed (ω) and motor input current (I_{motor}). In this way, the torque into and out of the gearbox is known when the configuration in fig. 7 is used, and the gearbox efficiency can be determined.

Figure 6. Cut-away drawing of wind turbine tower gearbox with rotor attached.

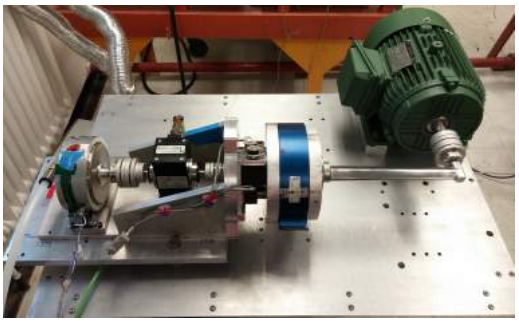

Figure 7. Test rig for determining gearbox efficiency.

The motivation for using this methodology is that the current setup cannot directly measure the motor output (gearbox input) during a gearbox test. The characterization and mapping process, completed a-priori to a gearbox test, ensures that the efficiency can be quantified. Using this technique requires generating a surface map with the functional form:

$$\tau_{motor} = fit(\omega, I_{motor}) \tag{2}$$

(here a linear interpolant was chosen as the fit for simplicity) from which the motor torque can be queried for any run condition. For the AC motor used in these experiments, low motor speeds and low motor current levels produce unacceptable scatter in the motor output prediction. Therefore, to improve the surface fit, a cutoff was set at $I_{motor} > 1.3$ (A) and $\omega > 2250$ (RPM). The resulting map is shown in figure 8.

Following the motor characterization, a series of tests were conducted on several gearboxes of identical design by applying various braking loads at multiple test speeds until gearbox failure. These data were then filtered so that the input torque could be predicted using the surface map in figure 8, and the efficiency calculated via:

$$Efficiency = \epsilon = \frac{\tau_{measured}}{\tau_{motor}} \tag{3}$$

This data is shown in figure 9 as a function of measured speed. Error-bars are shown only for standard deviation of the measured speed and torque, and are much larger than the sensor accuracy. Note that over 540 individual data points were taken during these tests, and only 18 are available to determine the efficiency. The reason for this is the gearbox design itself. Due to the previously discussed geometrical constraints on the system, the original design called for a maximum torque capacity of 1 (Nm). Above this level the gearbox lifetime is dramatically

shortened. The unexpected scatter in the AC motor data at low speeds and low input currents precludes the use of this method for predicting the gearbox efficiency outside of the threshold shown (determined by the surface fit of the motor output and range of the available data points.) In this regime we conservatively find the gearbox efficiency to be:

$$\epsilon = 85\% \pm 15\% \quad \texttt{for } 0.93 < \tau < 1.35 \ (Nm) \ \texttt{and } 2725 < \omega < 3480 \ (RPM) \tag{4}$$

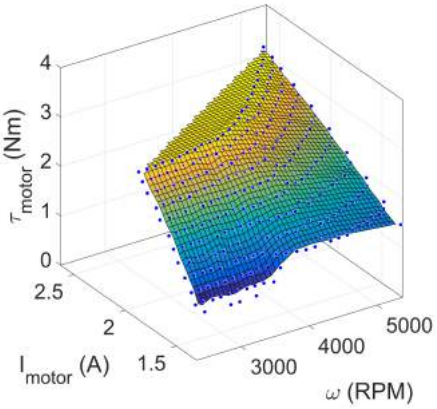

Figure 8. Linear surface interpolation map for finding torque output by AC motor, before entering gearbox.

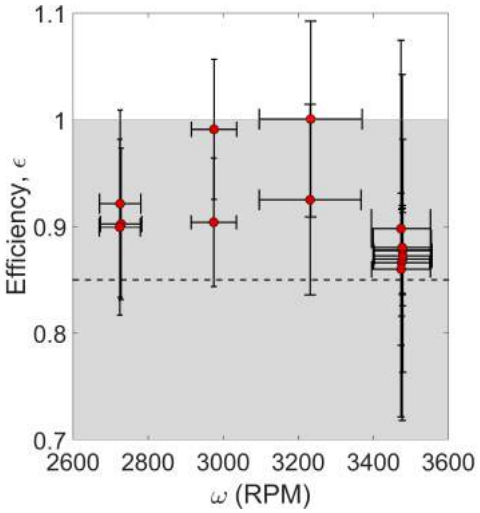

Figure 9. Efficiency estimate from gearbox testing. Error-bars show ±1 standard deviation of the measured speed and torque values. Dashed black line is the final efficiency of equation 4, with shaded regions showing range of uncertainty.

Note that this is a broad range, and further work is being completed to narrow the uncertainty of the gearbox by adding a second torque transducer before the gearbox so that input and output torque can be measured directly. This correction for gearbox losses does not have any dependency on the input speed or torque levels, both of which may play a crucial role in the true value of ϵ. Furthermore, the mean efficiency correction of 85 % is low compared to values found in the gearbox literature [14], which are typically around $\epsilon = 98\%$ for right-angle bevel gearboxes. As previously noted, this particular design was tested outside its design limit (see section 2.3), and most likely contributed to the low efficiency level.

4. Power Coefficient

The power coefficient is shown in figure 10 with no corrections applied. A range of Reynolds numbers were tested, from $Re_D = 5.3 \times 10^6$ to 9.7×10^6. For each value of the Reynolds number, the tunnel pressure and free-stream velocity are fixed. The turbine braking load is then varied to change the rotational speed, and thus TSR. The shape of each power curve remains consistent for all runs, and the peak power coefficient occurs at the same TSR for each data set. There is some scatter in Reynolds number, and no clear trend is evident. This may be explained by a changing gearbox efficiency. However, for all tests shown, the correction found in the previous section is not strictly applicable as it does not fall within the bounds set in equation 4. In these initial tests, the torque measured was considerably lower than $\tau = 0.93$. Much of the data

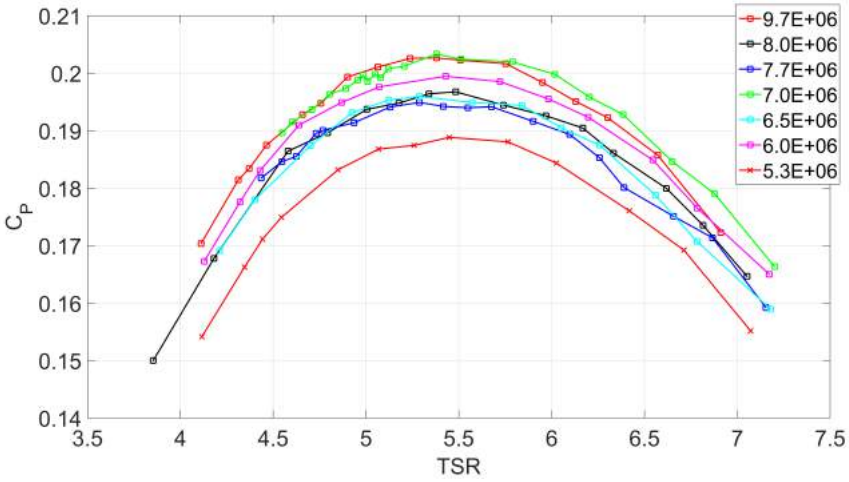

Figure 10. Power coefficient with no corrections applied as a function of tip speed ratio for various Re_D. Note that the gearbox used was the same for all runs.

does fall within the limitations on ω and the correction may be applied assuming it is torque independent. This is shown in figure 11. The uppermost bound represents an increased gearbox loss of 70% while the lower bound is for an ideal gearbox with no losses. It is important to note that all data shown here was acquired with the same gearbox. This would indicate that the efficiency should remain constant for a given input ω and τ. However, different tunnel densities and free-stream velocities were used for all of these tests so that the aerodynamic τ and ω are not constant. If the gearbox correction does change its functional form based on input torque and rotational speed this would account for the scatter in Reynolds number.

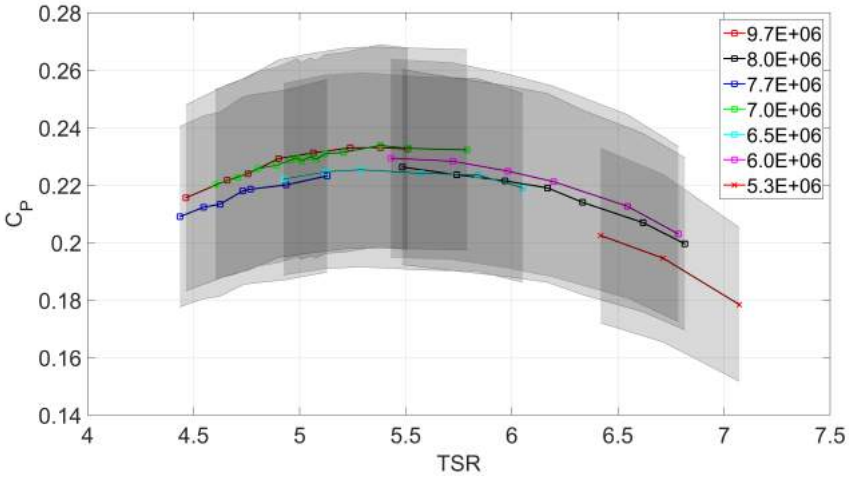

Figure 11. Power coefficient with the correction in equation 4 applied. Only data sets which fall within $2725 < \omega < 3480$ (RPM) have been used while neglecting the limitation on torque $(\tau > 0.93\ (Nm))$.

The uncertainty in the correction is currently much larger than any of the measurement errors due to instrumentation accuracy or random noise. The correction does imply that there

may be a trend in Reynolds number, but any conclusions are obfuscated by the uncertainty of the efficiency. The lower than expected values of C_p, even when considering the somewhat crude correction, can also be attributed to a less than ideal rotor design. In particular, the 35% thickness airfoil chosen near the hub makes generating lift and drag curves for a Blade Element Momentum (BEM) simulation difficult. In addition to reducing the uncertainty in the gearbox efficiency, current work is ongoing to measure the lift and drag coefficients experimentally at matched Reynolds numbers. This will allow for convenient and accurate comparisons of the experiments with BEM simulations.

5. Conclusions

The first set of experiments have been completed at near full-scale Reynolds numbers and matched Tip Speed Ratios for a model wind turbine. Issues concerning the design and efficiency of the turbine gearbox are discussed. A correction for losses within the gearbox was found for a narrow range of operating conditions, and current work is ongoing to improve the range and accuracy of the measured efficiency. Finally, initial measurements of the power coefficient are provided for a range of Re_D values.

6. Future Work

More accurate measurements of the gearbox efficiency are necessary in order to draw conclusions about the behavior of the power coefficient as a function of Reynolds number. Work is underway to determine the value of ϵ as a function of speed and input torque. Furthermore, a new gearbox design is being developed for the highest Reynolds number experiments. Near-future activities will focus on resolving the issues with the thrust measurements so that comparisons with BEM can be made which are independent of the gearbox efficiency. Following this, work will begin on resolving the wake velocity profile in the streamwise direction using both pitot-static tubes and hot-wire anemometers so that the scaling with Reynolds number can be further investigated.

Acknowledgments

The authors wish to acknowledge the funding agency for this work, a National Science Foundation grant (NSF CBET-1435254, program director Gregory Rorrer). There was also considerable technical assistance provided by Dan Hoffman and Glenn Northey. Finally, thanks is due to Professor Martin O.L. Hansen for helpful feedback on the experiment and various theoretical considerations.

References

[1] Adaramola M and Krogstad P 2011 *Renewable Energy* **36** 2078–2086
[2] Vries O D 1983 *Annual Review of Fluid Mechanics* **15** 77–96
[3] Vermeer L, Sørensen J and Crespo A 2003 *Progress in Aerospace Sciences* **39** 467–510
[4] Snel H 1998 *Wind Energy* **1** 46–69
[5] Simms D, Schreck S, Hand M and Fingersh L 2001 NREL unsteady aerodynamics experiment in the NASA-Ames wind tunnel: A comparison of predictions to measurements Report TP-500-29494 National Renewable Energy Lab
[6] Schepers J and Snel H 2007 Model experiments in controlled conditions Report ENC-E-07-042 ECN
[7] Jiménez J M, Reynolds R and Smits A J 2000 Preliminary velocity measurements in the wake of a submarine model *APS Division of Fluid Dynamics Meeting Abstracts* vol 1
[8] Jiménez J M, Hultmark M and Smits A J 2010 *Journal of Fluid Mechanics* **659** 516–539 ISSN 1469-7645
[9] Ashok A, Van Buren T and Smits A 2015 *Journal of Fluid Mechanics* **774** 416–442
[10] Vallikivi M, Hultmark M and Smits A 2015 *Journal of Fluid Mechanics* **779** 371–389
[11] Reynolds R M 1953 Preliminary results of an investigation of the effects of spinner shape on the characteristics of an naca d-type cowl behind a three-blade propeller, including the characteristics of the propeller at negative thrust Tech. rep. DTIC Document

[12] Marten D, Wendler J, Pechlivanoglou G, Nayeri C and Paschereit C 2013 *International Journal of Emerging Technology and Advanced Engineering (IJETAE)* **3** 264–269
[13] Shigley J E, Budynas R G and Mischke C R 2004 *Mechanical engineering design* (McGraw-hill)
[14] Radzevich S P and Dudley D W 1994 *Handbook of practical gear design* (CRC press)